Scanning Tunneling Microscopy Study of Titanium Oxide Nanocrystals Prepared on Au(111) by Reactive-Layer-Assisted Deposition

Denis V. Potapenko,[†] Jan Hrbek,[‡] and Richard M. Osgood[†,*]

[†]Department of Applied Physics and Applied Mathematics, Columbia University, New York, New York 10027, and [‡]Chemistry Department, Brookhaven National Laboratory, Upton, New York 11973

ABSTRACT We report on an scanning tunneling microscopy study of the nanocrystallite phases of TiO_2 formed *via* reactive-layer-assisted deposition in ultrahigh vacuum. The synthesis used reaction of a thin layer of water, on a Au(111) substrate at 130 K, with low-coverage vapor-deposited Ti. The effects of annealing temperature and reactant coverage were investigated. Large-scale (>20 nm) patterns in the surface distribution of nanoparticles were observed with the characteristic length-scale of the pattern correlating with the thickness of the initial layer of H_2O. The phenomenon is explained as being due to the formation of droplets of liquid water at temperatures between 130 and 300 K. After the surface was annealed to 400 K, the individual titania nanoparticles formed by this process had diameters of 0.5—1 nm. When the surface was annealed to higher temperatures, nanoparticles coalesced and for annealing temperatures of 900 K compact nanocrystals formed with typical dimensions of 5—20 nm. Three distinct classes of nanocrystallites were observed and their atomic structure and composition investigated and discussed.

KEYWORDS: nanoparticles · TiO_2 · titania · reactive-layer-assisted growth · Au(111)

Freestanding "nano-objects," such as colloidal quantum dots and nanoclusters, are of interest because of their potential applications as light emitters, solar collectors, and catalysts and because of their interesting fundamental material properties such as size-dependent electronic structure and excitation energies. The rapid growth of nanoscience has been fueled in part by the many new preparative techniques developed for the growth and probing of such nano-objects. Synthesis of composite (*i.e.*, consisting of more than one element) nano-objects poses a particular difficulty because of an additional variable, that is, stoichiometry. Despite significant advances, ultrahigh-vacuum studies of the fundamental surface properties of these objects are still in the early stages. Such studies are particularly important to achieve a rigorous understanding of their chemical activity or their properties as charge-transfer media. The most common method of preparation of these nanocrystals is *via* colloidal growth. However, a particular difficulty in investigating surface reactions on these colloidal-grown nano-objects under well-defined conditions is the preparation of a pristine surface following synthesis. For example, free-standing quantum dots are typically prepared with surface terminating groups, such as TOPO (trioctyl phosphine oxide) for CdSe dots or oleic acid for ZnO; full removal of these groups is extremely difficult under ultra high vacuum (UHV) conditions.

As a result, several groups have adopted *in situ* nanoparticle-preparation methods in conjunction with a dedicated scanning tunneling microscope (STM) probe. In principle, this approach allows examination of nanoparticle structure during particle synthesis or during subsequent stages of reaction. *Composite* nanoparticles can be synthesized in UHV using several related processes that rely on vapor deposition and surface reactions. Thus, Helveg *et al.*[1] have grown MoS_2 nanoparticles by depositing Mo on Au in presence of H_2S at a substrate temperature of ~400 K. Within a certain range of parameters, this method yields an ordered thin film; in fact, Guo *et al.*[2] and Männig *et al.*[3] reported growing well-ordered TiO_2 thin films by depositing Ti in O_2 on Mo(110) and Ru(0001), respectively, at 600 K. A variant of this approach is to first form a *chemisorbed* layer of one reactant and then deposit a second reactant on the chemisorbed layer so as to reactively form compound nanoparticles. Cai *et al.*[4] and Biener *et al.*[5] have successfully used this method to prepare RuS_2 and TiS_2 nanoparticles, respectively, on Au substrates. Recently very promising results have been

*Address correspondence to osgood@columbia.edu.

Received for review March 19, 2008 and accepted May 23, 2008.

Published online June 20, 2008.
10.1021/nn800169y CCC: $40.75

obtained with a similar approach for the case of TiO_2 using oxidation of deposited Ti islands.[6,7] In the third variant of the reactive layer approach, termed reactive-layer-assisted deposition (RLAD), a *physisorbed* multilayer of one reactant is first deposited on a substrate and the second reactant (metal) is then physical-vapor deposited onto this layer. In this case the metal atoms react with the loosely bound molecular multilayers at relatively low temperatures. Raising the substrate temperature causes any unreacted, adsorbed molecules to desorb from the substrate surface; the final product compound is then left on the surface in the form of an ensemble of nano-particles. RLAD has been used successfully to form nanoparticles in a variety of materials systems. Specifically, Horn *et al.*[8] used Mo reactions with C_2H_4 multilayers and Kim *et al.* used O_2 to react with Mg[9] and Au,[10] thus forming MoC_2 and MgO and Au−O nanoparticles, respectively. In these and several of the above experiments single-crystal Au was used as a substrate owing to its relative chemical inertness; in addition, the surface structure of Au crystal was useful in elucidating the substrate's template effects. In RLAD, it is possible, in principle, to use the thickness of a reactive multilayer to tune the size of the nanoparticles; this thickness tuning is similar to variation in nanoclusters size achieved in the method of buffer-layer-assisted growth (BLAG).[11] Note, however, that these two methods are different: in the latter method the buffer layer only physically interacts with the deposited metal, while in RLAD the reactive layer also has chemical interaction with the metal, supplying one elemental constituent to the nanoparticle formation.

Prior work in our laboratory characterized in a preliminary way the chemical, structural, and electronic properties of TiO_2 nanocrystals grown *via* RLAD using X-ray photoelectron spectroscopy (XPS), STM, and scanning tunneling spectroscopy (STS).[12] These experiments showed that ~1 nm diameter TiO_2 particles, formed with an H_2O reactive layer, could be obtained after raising the substrate temperature to 300 K. Similar results were obtained when a NO_2 reactive layer was used except, in this case, the titanium was fully oxidized to TiO_2 even at cryogenic temperature. This UHV-compatible method for preparing well-defined TiO_2 nanoparticles can be used, for example, in molecular-level studies of reaction mechanisms of photocatalytic processes on TiO_2 nanoparticle surfaces.

The present paper reports on a more extensive investigation of this approach for the growth of TiO_2. In particular, we report on the use of STM methods to determine the influence of the reactive layer thickness on the areal and size distributions of the nanoparticles. Also we study the thermal stability and evolution of these particles and derive the atomic structures of the most stable crystallite structures.

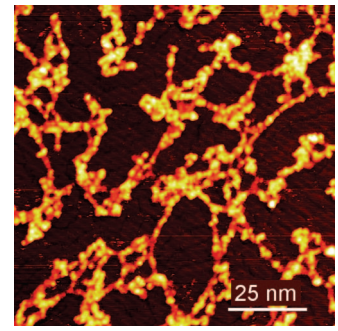

Figure 1. STM image of an Au(111) surface with TiO_2 nanoclusters prepared by deposition of 0.2 ML of Ti on a 10 ML thick layer of H_2O on a Au(111) substrate at 130 K, followed by annealing to 400 K. Size of the image = 100 nm × 100 nm.

RESULTS AND DISCUSSION

Summary of Chemical Composition of RLAD-Formed Titanium Oxide Nanoparticles. In previous work[12] we reported on XPS studies of the oxidation states of TiO_x upon deposition of 0.1 ML of Ti on ~30 ML of water on the Au(111) surface at 90 K followed by annealing. (In this work we define 1 ML as the density of Au atoms on a Au(111) surface that equals to 1.4×10^{15} cm^{-2}). These studies showed that immediately after deposition Ti is present in several oxidation states but after annealing to 300 K only the bulk TiO_2, that is, Ti^{4+}, state is observed. In addition, O 1s core-level spectra were obtained from the same surface; in general the core-level shifts could also be identified with the fully oxidized titanium state. However, note that at lower temperatures and prior to the formation of TiO_2, the O1s spectrum had a significant contribution from an intermediate state most likely corresponding to oxygen with Ti−OH coordination;[12] this contribution became negligible upon heating to 300 K. The fully oxidized state was found to be pervasive in all particles prepared after heating to room temperature. Therefore, in the present work it is assumed that the nanoparticles produced in the experiments described below have the bulk TiO_2 stoichiometry. However, in the section to follow on octagonal crystallites we discuss the possible incorporation of hydrogen during nanoparticle formation.

Nanoparticles Formed at Low Annealing Temperature. Figure 1 shows an STM image of TiO_2 nanoparticles prepared on a Au(111) surface by deposition of 0.2 ML of Ti on ~10 ML of ice at 130 K, followed by annealing for 5 min at 400 K. Titania nanoparticles of 0.5−1 nm in size are formed in complex patterns on the surface. Considering a typical atomic volume for rutile of ~10 $Å^3$ per atom, each of these particles consists of 10−50 atoms. The particles do not show any preferred shape or orientation with respect to the substrate nor do they register with the underlying herringbone reconstruction of the Au(111) surface. For comparison, pure Ti deposited on Au(111) at room temperature has been shown to nucleate at the elbows of the herringbone

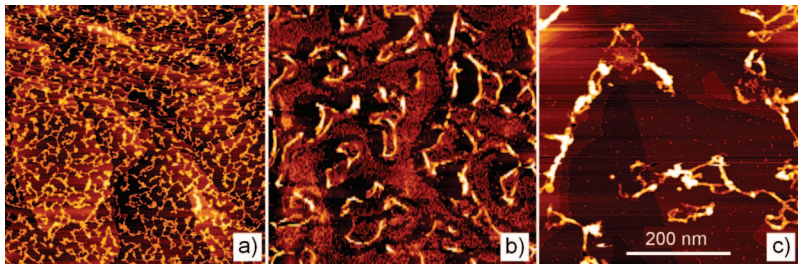

Figure 2. STM images of surfaces prepared by the same procedure as that in Figure 1 but with different initial thickness of water layer: (a) 10, (b) 60, (c) 300 ML. Size of all images 500 nm × 500 nm.

structure and to yield Ti islands with an identical height, corresponding to one atomic layer.[6] Thus our observations of the lack of preferential-site location implies that our nanoparticles are formed in the water layer out of contact with the gold substrate. This conclusion is also supported by the previous XPS data showing that the titanium is oxidized upon deposition at 90 K.[12]

The details of the patterns formed from the particles depended on the water coverage prior to deposition. Figure 2 shows three 500 nm × 500 nm STM images of surfaces prepared under nearly identical conditions with varying water layer thickness, namely 10, 60, and 300 ML. Curved ridges consisting of bunched TiO_2 nanoparticles are a typical feature of the particle surface distribution. The changes in the patterns in going from image a to image c show clearly the dependence of their characteristic pattern dimensions on initial water-layer thickness. Specifically, the lateral dimensions of the pattern, that is, the typical distance between adjacent ridges, are 20, 100, and 300 nm, while the maximum height of the ridges are 1, 4, and 7 nm for the images a, b, and c, respectively. To explain this observation we postulate the formation of liquid water droplets as an intermediate stage prior to the evaporation of water, as discussed in the next paragraph.

First, we need to establish the state and morphology of the water layers grown in our experiments at 130 K. Water vapor deposited on substrates at temperatures below 145 K is known to form a metastable amorphous solid water (ASW) phase.[13,14] Considering morphology, it was shown that at 100 K water forms a continuous single layer on Au(111) before the onset of cluster formation[15] and at 108 K water deposition results in the formation of smooth multilayers of ASW up to 14 nm thick.[16] At higher temperatures the transformation of ASW to crystalline ice (CI) occurs; specifically, at 155−160 K the transition proceeds on the time scale of seconds[13,17,18] and at 135 K it takes >500 min for the complete transformation of a 14-nm-thick ASW layer.[16] This transition involves the supercooled liquid water[18] intermediate, and, as a result of hydrophobic nature of Au(111) surface,[19,20] uniform films of AWS are transformed into arrays of three-dimensional clusters of CI on a partially exposed substrate.[13,16] (Although bulk water is unstable in its liquid state under UHV conditions, there is a large body of both experimental[18,21] and theoretical[22] work that reports the existence of supercooled liquid water in thin layers on surfaces.) Since in each of our experiments the deposition of water and titanium was performed within a time period of ~10 min at the sample temperature of 130 K, it is reasonable to assume that water formed relatively flat layers of ASW. Yet, since the vapor deposition and the ASW to CI phase transition are kinetically very different processes, we cannot exclude, on the basis of prior research, the possibility that water deposited on the sample at 130 K produces large three-dimensional clusters of CI and part of Au(111) surface remains exposed. Note, however, that there is no evidence of the latter mode of water film growth in our experimental data.

Liquid water formation at ~155 K is important for the explanation of our observed surface distribution of the nanoparticles (as shown by Figure 2). A sketch of the processes, which can explain the origin of the experimentally observed surface distribution of TiO_2 nanoparticles, is shown in Figure 3. Here we assume that at an intermediate temperature before complete evaporation (*e.g.*, above 180 K) water forms nanodroplets of liquid. This formation is then followed by a complex combination of evaporation and convection of liq-

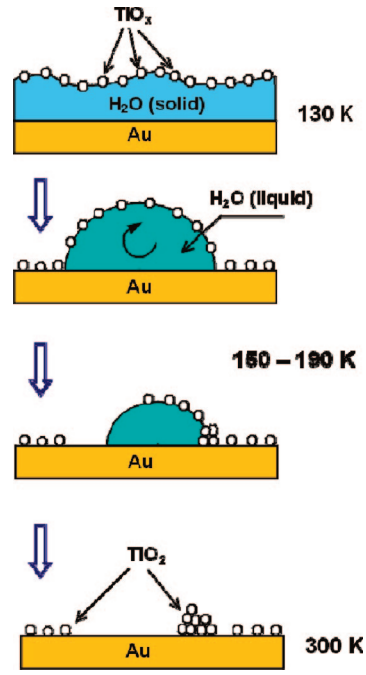

Figure 3. Schematic explaining the formation of the large-scale patterns of TiO_2 nanoclusters using liquid water intermediate.

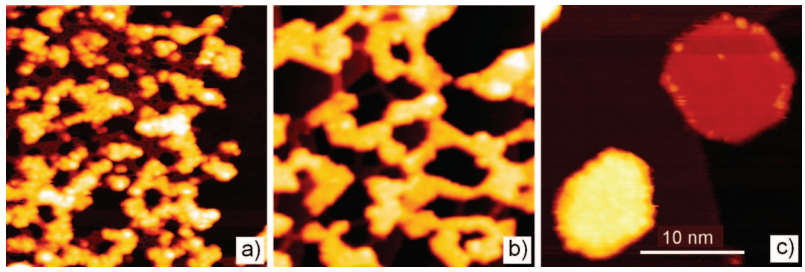

Figure 4. Thermal evolution of titania nanocrystals. STM images of a surface prepared by the same procedure as in Figure 1 with 60 ML of water and annealed to: (a) 400, (b) 600, and (c) 900 K for 5 min in each case. Size of all images: 25 nm × 25 nm.

uid inside the droplets,[23] which creates the observed ridges and the areas void of nanoparticles. Similar agglomeration of vanadia nanoparticles was observed when they were prepared by deposition on water multilayers.[24] In addition, a liquid-water model was invoked to explain the distribution of Ag nanoparticles prepared by physical vapor deposition on ice multilayers on a HfO_2 surface.[25]

Thermal Evolution of Titania Nanoparticles. Below the annealing temperature of ~400 K, the surface structures are too unstable for scanning and the STM-probe/surface interactions lead to frequent tip crashes during the scanning process. Figure 4 shows STM three images of identical size, that is, 25 nm × 25 nm, prepared by deposition of 0.2 ML of Ti on 60 ML of ice and followed by consecutive annealing steps to (a) 400, (b) 600, and (c) 900 K. After annealing to 400 K the nanoparticles appear as disordered aggregates of particles with typical vertical and horizontal dimensions both being ~0.5 to 1 nm. Note that the images do not provide reliable information on the shape and orientation of individual nanoparticles as they are smaller than the typical radius of an STM tip. After annealing to 600 K for 5 min local atomic rearrangement of the particles occurs, with a characteristic scale length of 5 nm. As a result of this annealing, crystallites are formed with flat top faces, 1−3 nm in width and 0.6 nm in height (Figure 4b). No periodic atomic arrangement on the top faces could be discerned in the STM images. Subsequent annealing to 900 K causes long-range redistribution of material, thus resulting in compact, ordered structures forming on the surface (see Figure 4c). An examination of the surface distribution of nanostructures formed after annealing to 900 K for 5 min shows that the diffusion length for the TiO_2 nanoparticles is ~50 nm at this temperature.

Figure 5 exhibits three STM images of the surfaces shown in Figure 2 after subsequently annealing to 900 K for 5 min. The images show that high-temperature annealing of the nanoparticle aggregation, which was formed with a relatively *thin* initial water layer (10 ML, Figure 2a), produces an array of compact nanoislands evenly distributed across the surface (Figure 5a). The size distribution is relatively narrow ranging from 5 to 15 nm. In contrast, nanoparticles formed from thick initial adlayers of water, that is, 300 ML, had the large-scale particle arrays shown in Figure 2c. These arrays still retain the size and geometry of the original pattern (Figure 5c) after high temperature annealing. Apparently, the ridges, which consist of conglomerates of nanoparticles, are transformed by annealing into solid formations of irregular shapes. Note that on a larger spatial scale these formations resemble the shapes of original ridges. For nanoparticles prepared with 60 ML of water (Figure 2b), that is, an intermediate water layer thickness, annealing creates both compact islands and elongated ridges (Figure 5b). The above observations suggest that to prepare TiO_2 nanoparticles with the most uniform size and shape distribution, one should use the thinnest layer of water that is sufficient for complete oxidation of the deposited titanium. Thus comparatively good quality crystallite distributions can be obtained with 10 ML of water and 0.2 ML of titanium.

Atomic Structures of Titania Nanoparticles. Next we explore the atomic structures of individual TiO_2 nanoparticles prepared with low values of initial water coverage (10 and 60 ML) and by annealing to 900 K for 5 min. The analysis of our STM images allows us to identify three basic classes of nanoparticle structures: hexagonal crystallites, 3-dimensional crystallites, and octagonal crystallites. Although the majority of the compact objects formed on the surface after annealing had irregular shapes, each object could, in general, be assigned to one of the three classes on the basis of specific characteristic features. Each of these different structures occurred with a relative abundance that depended on water and titanium coverage during preparation. Below we discuss each of the observed structures in detail.

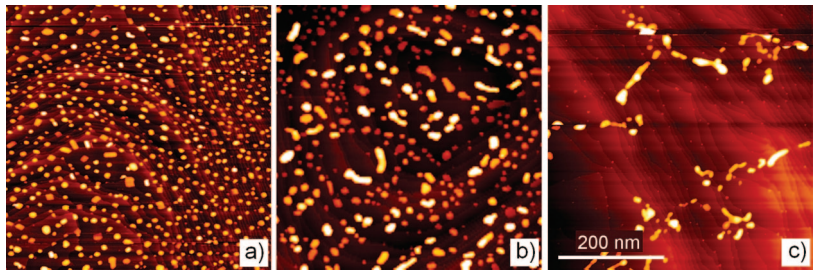

Figure 5. STM images of the same surfaces as in Figure 2 panels a, b, and c, respectively, after annealing to 900 K for 5 min. Size of all images 500 nm × 500 nm.

Hexagonal Crystallites. The most abundant nanocrystal type, which accounts for an estimated ~60 to 75% of the titania by volume, has a distinctive hexagonal appearance (see, for example, the lower object in Figure 4c). These crystallites are flat structures with a width of 5−20 nm and with a height of 0.6−1.8

nm. The edges of these crystallites tend to align along the close-packed ⟨110⟩ directions on the Au(111) surface although some crystallites remain irregular in shape. Fully formed crystallites have the perfect hexagonal shape seen in Figure 6a; however, irregularly shaped crystallites are also formed, as seen in Figure 6b. The top faces of the nanocrystals are parallel to the surface plane. When the STM tip was used to apply a lateral force to a nanoparticle, the hexagonal crystallite was horizontally displaced without change in its shape and without any damage to the Au(111) substrate. This observation suggests that hexagonal crystallites lie fully on top of an otherwise undisturbed Au(111) surface and are only weakly bound to the substrate. The adatom patterns on the top face of the crystallites have a corrugation of ~0.2 nm that makes them appear "rough" in the STM images. These patterns are often irregular but sometimes contain periodic rows of adatoms (Figure 6a). In the latter case the spacing between these rows is 0.90−0.95 nm and the rows are always parallel to ⟨11–2⟩ directions on the Au(111) surface, that is perpendicular to one of the edges of the crystallite. Occasionally a two-tiered hexagonal crystallite (Figure 6b) was observed. Since to a good approximation the electronic density of states of the top-layer should be nearly the same as that of the bottom layer, this structure can be used to determine the height of a single atomic layer. This measurement gave a height of 0.23 ± 0.01 nm. By comparison our measured values for the thickness of the typical-thickness of the hexagonal crystallites, with respect to the Au substrate, were never smaller than 0.55 nm, suggesting that the thermodynamically stable hexagonal structure comprises at least two atomic layers.

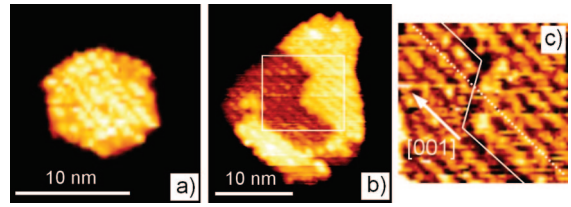

Figure 6. STM images of hexagonal crystallites: (a) A fully formed hexagonal crystallite; image size, 17 nm × 17 nm; (b) an irregular hexagonal crystallite with two-layer structure on the top face; image size, 25 nm × 25 nm; (c) "zoom in" of the marked area in image b. The grayscale shows the local height of the data points. The solid line marks the position of the step edge. The dotted line demonstrates the registry relationship between the two layers: it marks the position of a ridge in the top terrace (in the right side of the image), but it runs between a ridge and a trough of the bottom terrace (left side). Crystallographic directions in Figure 6c are that of the proposed rutile(100) structure of the crystallites.

To relate our STM-derived geometrical parameters with known atomic structures of TiO_2 (rutile and anatase), we examined the known crystallography of TiO_2; (see comprehensive review by Diebold of titania surface structures).[26] This comparison allows us to propose rutile with its (100) plane parallel to the substrate as the basic atomic structure of the hexagonal crystallites. Observations that support this assignment are, first, that the known single atomic-layer height for rutile(100) is 0.229 nm; this value is essentially identical to the value of 0.23 ± 0.01 nm as measured in our experiments. Second, the measured spacing between rows on the top faces of the crystallites is 0.90−0.95 nm. This value appears to correspond to the (1 × 2) reconstructed rutile(100) surface, which would have 0.916 nm periodicity. Third, we note that the rows on two adjacent rutile(100) (1 × 2) layers are parallel but shifted by 0.229 nm, that is, $^1/_4$ of the row spacing. This value is not inconsistent with our observations; see the dotted line in Figure 6c. The first observation is compelling because no other known titania structure has a layer thickness close to 0.23 nm. With respect to the second observation, it should be mentioned that only (1 × 1) and (1 × 3) reconstructions have been seen on bulk rutile(100) surfaces.[27] However, influence of the substrate due to the monolayer-scale thickness and flat orientation of the crystallites may alter the physical properties of TiO_2 making the (1 × 2) reconstruction favorable. Also, the possibility of gold atoms arranged in a (1 × 2) overlayer on the rutile(100) surface cannot be ruled out.

Given the proposed orientation of rutile(100) crystallites, the two edges of (fully formed) hexagonal structures, which are perpendicular to the adatom rows, would be parallel to ⟨010⟩ directions of the rutile lattice. The other four edges would belong to ⟨013⟩ group of directions. Indeed, the angle between [010] and [013] directions in rutile structure is 62.6°, which is close to the 60° angle of the edges on our hexagonal crystallites. For surface bound crystallites the orientation of the edges will not be determined solely by the thermodynamics of the crystallites but also by crystallite-substrate interactions. The edges of the top layer of the hexagonal structure, shown in Figure 6b,c, that are not in contact with the Au(111) substrate, tend to run in the [001] direction of rutile(100). This edge feature is not seen for the external edges of the crystallites that are in contact with the substrate. The observed alignment of the external edges may be due to anisotropy in diffusion kinetics of TiO_2 on Au(111), as reported elsewhere.[6,28]

Similar hexagonal formations have been observed when TiO_2 nanoparticles are formed on Au(111) by different methods.[6,7,12] In particular, hexagonal crystallites were reported in an experiment, in which TiO_2 was prepared by deposition of Ti at room temperature (RT) on Au(111), followed by oxidation in O_2 also at RT, and then annealed to 900 K.[6] Hexagonal crystallites have also been observed using RLAD with NO_2 on Au(111) and vacuum annealed to 700 K.[12] In both of these cases, crystallite edges were aligned to the ⟨110⟩ directions and patterns of adatoms on the top face were visible in the STM images. Despite these similarities, there are certain differences between hexagonal crystallites

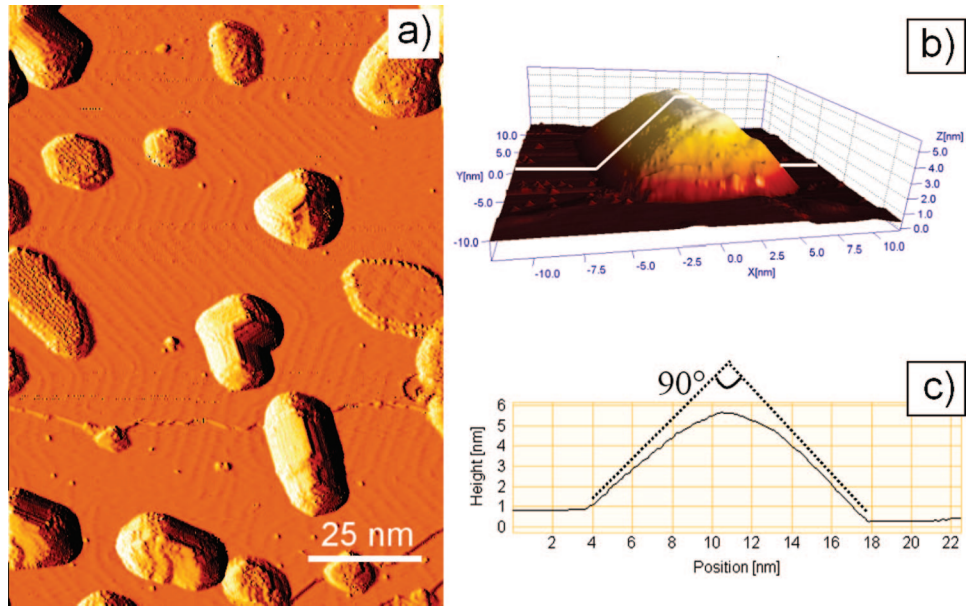

Figure 7. (a) Differentiated STM image of Au(111) surface with TiO_2 nanocrystals prepared by deposition of 0.2 ML of Ti on 60 ML thick layer of H_2O on a Au(111) substrate at 130 K, followed by an anneal to 900 K. Ridge-like formations are seen in the center. Size of the image 100 nm × 130 nm. (b) 3D rendering of the image of one of the ridge-like crystallite. (c) Profile of the crystallite in panel b as marked by the white line.

formed by different methods. The TiO_2 islands prepared by O_2 oxidation of Ti on Au(111) had an apparent height of 0.3 nm at a bias of +2.5 V,[6] a value also used in our studies; however, in the present work the minimum height of the crystallites was 0.55 nm. We will examine this difference in more detail in a separate paper, which will describe preparation of TiO_2 through O_2 oxidation of a Ti/Au surface alloy. Another difference in the structure of our crystallites lies in the atomic patterns on the top face of the crystallites. Previous reports have described periodic patterns with 1.4 and 2.4 nm,[6] and 0.46, 0.37, and 0.30 nm spacing.[12] In the present study, if any regular pattern could be discerned, it had a consistent 0.90−0.95 nm periodicity.

3D Crystallites. The second common nanocrystal type observed on Au(111), after annealing TiO_2 particles to 900 K, was a three-dimensional structure, the characteristic features of which were comparable vertical and horizontal dimensions and the absence of a top face parallel to the surface. A number of such objects are seen in the center of Figure 7a. The crystallite near the bottom of Figure 7a, for example, measures 15 nm across and 4 nm in height. This type of crystallites is estimated to account for ~15 to 30% of the total RLAD crystal formation.

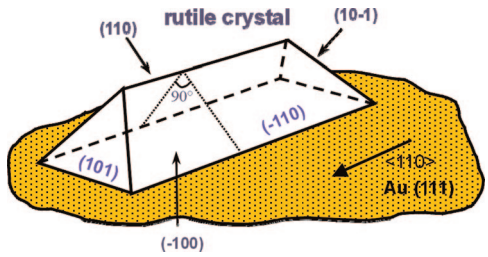

Figure 8. Schematic showing the proposed crystallographic orientation of the rutile structure that makes up a 3D-crystallite. Orientation of a Au(111) substrate is also shown.

Although many of these 3D crystallites have irregular shapes, most are ridge-like formations. These structures can be distinguished in the STM images by their characteristic "ridge" or top edge of the crystallite, which runs parallel to the substrate surface along one of the ⟨110⟩ directions on the Au(111) substrate. Sometimes two crystallites with different orientations coalesce and then the ridge shows a 120° bend as in the center of Figure 7a. The ridges are formed by two faces of a crystallite symmetrically oriented with respect to the substrate; see the three-dimensional rendering in Figure 7b and the cross-section in Figure 7c. The cross-section of this type of crystallite has side faces that are formed with an intersecting angle of ~90°. Unfortunately, due to finite tip curvature, STM images of high protruding objects are a result of convolution of the object by the tip. For this reason the roundness of the ridge of the crystallite could be a tip-induced effect.

Although morphological data alone is not sufficient for unambiguous identification of the nature of 3D crystallites, analysis of equilibrium crystal shapes of the bulk TiO_2 phases[29,30] suggests rutile as the most likely candidate for the 3D structures. In this case, the observed "ridges" would be formed by two adjacent (110) and (−110) faces of rutile and the interface between Au(111) and the crystallite formed by a (−100) plane, which is parallel to the surface, as shown in Figure 8. Note that in both the proposed atomic structures for hexagonal and 3D crystallites, the rutile(100) plane makes the interface with Au(111) surface. However, the orientation of the rutile crystallite is different in these two cases. In the case of the hexagonal crystal-

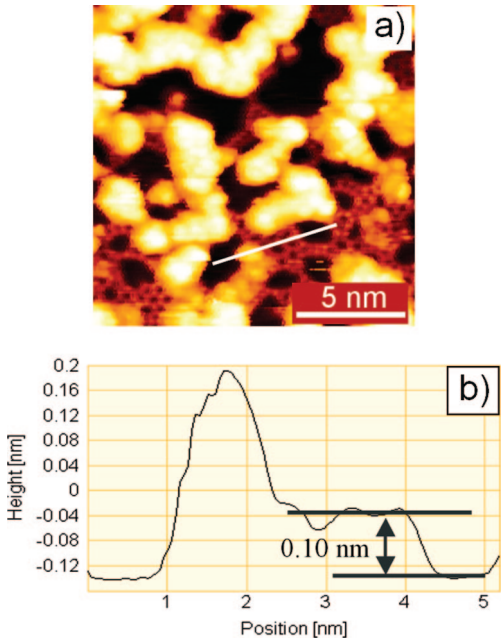

Figure 9. (a) STM image of the same surface as in Figure 2 b. Size of the image, 15 nm × 15 nm. Color scale emphasizes porous structure near the substrate. (b) Profile of the structure along the white line.

lites, the rows of Ti atoms in the [001] direction of rutile(100) are aligned parallel to ⟨11−2⟩ directions within the Au(111) surface, while in case of 3D structures they are parallel to close-packed ⟨110⟩ directions. This difference in orientation may be the cause of the observed two different morphologies of the titania crystallites.

Three-dimensional nanocrystal structures have been previously reported for the procedure, in which TiO_2 was prepared by O_2 oxidation[6] but the morphologies in this case—triangular, hexagonal, and needle-like shapes—were generally different from those reported here. From the point of view of nanocrystal symmetry, only the "needlelike" formations described in ref 6 are structurally close, if not identical, to the present 3D crystallites. Generally, the 3D
crystals here are much taller than those in ref 6 (6 *vs* 2.5 nm). This difference may be explained by the particular synthesis route in RLAD. In RLAD conglomerates of TiO_2 particles form upon water evaporation, as sketched in Figure 3, followed by fusion into single crystals at higher temperatures, a very different process than the simple Ti oxidation used in ref 6.

Octagonal Crystallites. The third crystal type is, for our synthesis conditions, much more of a minority structure; we estimate that only 5−10% of the structures fall in this category. This type of crystal, when fully formed, has octagonal symmetry as exemplified by the upper object in Figure 4c. The octagons appear to form *via* a very different route than the two crystallite types discussed above. The process of their formation is shown in Figures 9 and 10. Figure 9 shows an STM image of the same surface preparation as in Figure 4a (0.2 ML of Ti on 60 ML of H_2O, annealed to 400 K) but the chosen color scale emphasizes formations in the vicinity of the substrate. In addition, to the particles (white in the figure) corresponding to the TiO_2 nanoparticles and the Au(111) substrate (black), there is a complex two-dimensional pattern of pores in the vicinity of the particles. The position of these pores appears random and their size varies widely from 0.1 to 2.0 nm. Larger-scale images (*e.g.*, Figure 2b) show that the porous structure exists only in the immediate vicinity of TiO_2 crystallites (<5 nm) and is absent in areas devoid of the crystallites. The apparent height of the porous structure is uniform and is equal to 0.10 nm; see the cross section in Figure 9.

Annealing to higher temperatures caused morphological changes in the porous structures. In particular, after annealing of the surface in Figure 9 to 600 K the visible area covered by the porous structures became smaller; its patches grew more compact; and the pores became smaller (~0.5 nm), more uniform, and more ordered, as seen in the upper insert in Figure 10. Some patches show no pores, as in the lower insert in Figure 10. However these regions can be still identified by their characteristic apparent height of 0.10 nm. Further annealing to 900 K led to complete disappearance of the porous structure and formation of large crystallites. In addition to the hexagonal and 3D objects discussed above, a number of flat crystallites with octagonal shape were observed; see the upper object in Figure 4c. The apparent height of the octagonal crystallites varied, although they were generally <0.6 nm height. Their *minimum* height was ~0.10 nm; this coincides with the height of the porous formations and allows us to identify them as a thermodynamically stable form of the porous structure. Our experiments show that exposure of the surface to a flux of O_2, with the sample at 900 K, does not result in any change in the STM appearance of the octagonal crystallites, even after a 100 L exposure. For simplicity, in what follows we shall call all the structures belonging to this crystallite class "octagonal crystallites" irrespective of their actual crystalline shape.

The octagonal crystallites, when fully formed, had adjacent sides with a ~135° angle with respect to each other and with four sides, oriented at 90° to each other generally having a different length compared to the

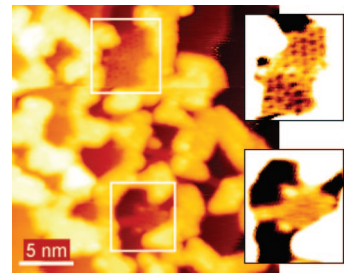

Figure 10. STM image of the surface in Figure 9a after 600 K anneal. The inserts show the marked areas with higher contrast. Size of the image, 25 nm × 25 nm.

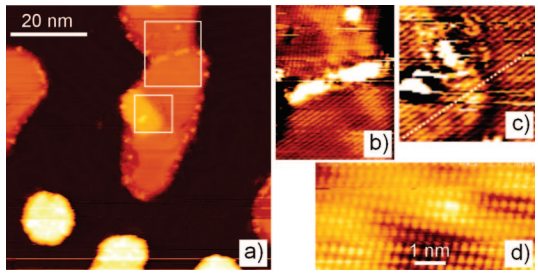

Figure 11. STM images of the surface in Figure 10 after a 900 K anneal. (a) Irregular-shaped octagonal crystallites; size of the image, 65 nm × 65 nm; (b) "zoom in" of the top marked area. Two structural domains can be seen. (c) "Zoom in" of the bottom marked area. The color scale shows the local height of the data points. The dotted line demonstrates that the structure of the top layer is in registry with that of the bottom layer. (d) Atomic-resolution STM image of the top face of an octagonal crystallite.

other four sides. The ratio of the lengths of their sides varied from 1:1 to 1:4 indicating that this ratio is not dictated solely by the thermodynamic parameters of the edges. Sizes of these crystallites lie in the 20−40 nm range. Unlike the hexagonal crystallites, the octagonal formations have very smooth top faces with some irregular corrugation, of order 0.02 nm, that is, comparable with the corrugation of the "herringbone" reconstruction on Au(111) surface. Typically, strings of adatoms could be seen along the perimeter of a crystallite. Fully shaped octagonal crystallites were usually formed in the areas with a high density of steps, while irregular octagonal crystallites were found mostly on large (>100 nm) terraces. This observation suggests that step flow on the Au(111) substrate at 900 K facilitates the mass transport responsible for shaping these structures into fully formed octagonal crystallites.

Figure 11a shows several irregularly shaped islands, which as judged from their height and appearance (that is, smooth top faces with 0.02 nm long-range corrugation surrounded by adatoms along the perimeter) of the top face, belong to the octagonal-crystallite class. At higher magnification, the top faces of the islands showed atomic-scale rows with 0.36 nm spacing (Figure 11b,c). In Figure 11b two domains of the octagonal structure are merged into one crystallite. Neither the atomic rows nor the edges of the (fully formed) octagonal crystallites were aligned along either the close-packed ⟨110⟩ or along the ⟨11−2⟩ directions on Au(111). Thus, in this case the octagonal crystallites had random orientation with respect to the Au(111) substrate.

It is well-known that the apparent height of objects in STM images cannot serve as measure of real physical height of these structures. However, as in the case of the hexagonal crystallites, the serendipitous appearance of a two-layer octagonal structure, such as shown in Figure 11 panels a,c, allows direct determination of the actual height of a single layer. In particular, the zoomed-in area of Figure 11c shows that the atomic structure of the irregular island and the small island on its top surface are identical suggesting the two layers have closely related or even identical similar electronic structures. Thus the measured height difference of 0.29 ± 0.03 nm provides a good estimate of the true single-layer height of the octagonal structure. Another observation from Figure 11c is that the atomic structures on the top and the bottom layers are in registry with each other, that is, a bright row in the top layer continues as also a bright row in the bottom layer (see the dotted line). The full atomic-resolution image of an octagonal crystallite (Figure 11d) shows a rectangular unit cell with the dimensions 0.36 ± 0.01 nm by 0.30 ± 0.01 nm. These dimensions were calibrated against an atomically resolved Au(111) surface in the same STM image.

The above atomic structure parameters allow us to identify the octagonal crystallites as lepidocrocide-like nanosheets of TiO_2 seen previously on Pt(111) surface (denoted as rect-TiO_2 phase)[31,32] and in freestanding form.[33] These earlier experiments used electron diffraction and STM measurements to find a 0.38 nm × 0.30 nm unit cell for this structure;[31,33] these atomic dimensions are very close to our observations. In addition, the earlier STM-derived height of a single layer of the structure was reported to be 0.25 nm;[31] that value is also in agreement with our measurements. The structure is, essentially, two parallel orthogonal lattices of Ti atoms pairwise connected by bridging O atoms within each lattice, as shown in Figure 12. In fact, it is the Ti atoms of the outward layer that are imaged as protrusions by the STM.[32] Oxygen atoms are displaced from the plane of Ti atoms so that the nanosheet is terminated by the bridging oxygen atoms on both of its faces. This oxygen termination leads to the weak structure−substrate interaction, manifested in our case in the apparent absence of the alignment of the octagonal crystallites with the substrate. Interestingly, this stable nanosheet formation is not unique for titania: identical atomic structure has been observed in the case of ultrathin vanadium-oxide films on Pd(111).[34] However, to the best of our knowledge, no prior work has reported on TiO_2 nanosheets on a Au(111) surface.

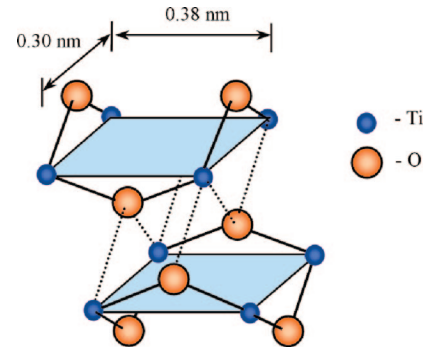

Figure 12. Unit cell of the atomic structure of octagonal crystallites (adapted from ref 33).

With regard to the origin of porous structures/octagonal crystallites, we note that these structures have not been previously reported for experiments using either O_2 or NO_2 as the precursor for titanium oxidation.[6,12] Apparently, the presence of hydrogen in the reactive layer may be important for the formation of this type of surface structure. Experiments using a combination of STM and TPD (thermal programmed desorption) probes, have shown that water adsorbs on a defect-covered TiO_2 rutile(110) surface both molecularly and dissociatively as OH.[35] Upon heating molecular water desorbs at ~290 K, and OH groups recombinatively desorb as H_2O at ~490 K.[35] Polycrystalline titania films show very similar behavior, with TPD peaks of H_2O occurring at 340 and 490 K for molecular and recombinative desorption, respectively.[36] In addition, it is known that titanium hydride TiH_2 decomposes at ~450 °C.[37] At the same time, experiments with vanadium deposited on water multilayers in an oxygen atmosphere have shown that, at room temperature, the resulting nanoparticles were composed of both vanadium oxide and hydroxide.[24] This hydroxide could be removed only by heating to 500 K, leaving vanadium in a lower oxidation state. The combination of the above experimental findings makes it reasonable to assume that in our experiments, surface titanium compounds are left in the form of both oxides and hydroxides after molecular-water desorption above 200 K, and only at higher temperatures is hydrogen removed. The origin of the pores could then be explained if a hydrogen-containing surface structure is formed at lower temperatures (*i.e.*, < 400 K) in the form of compact continuous islands on the surface. In this case, at ≥ 400 K, dehydrogenation would occur *via* the loss of H_2 and/or H_2O; this process would then lead to loss of volume, thus resulting in the formation of pores. At still higher temperatures (900 K), the consolidation of the porous structure would offer a pathway to TiO_2 nanosheet formation. It should be understood, however, that although the above tentative model appears to provide the best explanation for the observed phenomena, we do not have, as yet, direct experimental evidence supporting it.

CONCLUSIONS

In this paper, we have reported on the detailed structure and areal distribution of titanium oxide nanocrystallites formed by RLAD on Au(111). Our results show that the distribution and size of these crystallites depend on the thickness of H_2O layer and on the thermal treatment. The large-scale surface distribution of our titania nanocrystals suggests formation of liquid-water droplets in the RLAD process. Thus, the thickness of the reactive water layer should be minimized if one desires even distribution of nanocrystals on the surface. Three types of crystallites are seen after a surface with TiO_2 nanoparticles is annealed to 900 K: hexagonal crystallites are in majority; 3D "ridges" constitute a minority; and octagonal crystallites are found in low concentration. In the case of the first two types, their structure is that of rutile TiO_2. In addition, despite relatively weak oxide/metal-surface interactions most of the structures seen here are to some extent influenced in orientation by the Au(111) substrate. More generally, our results show that STM observations can be used to probe the formation of nanocrystals of metal oxides, to determine their crystallography, and to understand the characteristics of the process leading to their formation.

METHODS

The experiments discussed in the paper were conducted in a UHV chamber equipped with an Omicron VT-STM and a LEED/Auger system, sputtering gun, custom-built directed gas doser, and titanium-evaporation source. The base pressure in the STM chamber was 4×10^{-11} Torr. The standard Omicron sample manipulator was reengineered to allow direct temperature measurements of the sample with a K-thermocouple and to improve thermal contact between the sample and the liquid-nitrogen-cooling block. The lowest achievable temperature of the sample on the manipulator was 129 K.

All STM images were acquired at room temperature using W tips; the tips were prepared by a drop-off technique described elsewhere.[38] Each newly introduced tip was cleaned by heating with electron field emission at ~40 μA. Large-scale images (*i.e.*, 500 nm × 500 nm) were plane-corrected for better visual perception.

The Au(111) sample was prepared by cycles of Ar^+ sputtering (1 keV) and annealing at 850 K. Thinner reactive layers of H_2O (10 ML) were formed on the Au(111) surface by cooling the sample to 130 K and backfilling the chamber with water vapor to 1×10^{-8} Torr, as measured with an uncorrected ion-gauge, for 100 s. To calculate the reactive-layer thickness, unity-sticking probability of H_2O is assumed, which is a reasonable assumption at this sample temperature, and the ideal gas equations were used for the impingement-rate estimate. The thicker water layers were prepared using a directional doser to minimize the chamber-wall exposure to water vapor. The deposition rates were calibrated by a comparison of thermal programmed desorption peaks from surfaces prepared by backfilling the chamber with the desorption peaks measured using the directional doser. Titanium was physical-vapor deposited onto the reactive multilayer from a tungsten filament wrapped with titanium wire. The deposition rates of the Ti source were calibrated in prior experiments with a quartz-crystal monitor.

Acknowledgment. R. Osgood and D. Potapenko gratefully acknowledge support from the U.S. Department of Energy, Contract No. DE-FG02-90ER14104 and J. Hrbek from the U.S. Department of Energy, Division of Chemical Sciences, Contract No. DE-AC02-98CH10886. We wish to thank N. Zaki for help with the experimental setup and for helpful discussions.

REFERENCES AND NOTES

1. Helveg, S.; Lauritsen, J. V.; Laegsgaard, E.; Stensgaard, I.; Norskov, J. K.; Clausen, B. S.; Topsoe, H.; Besenbacher, F. Atomic-Scale Structure of Single-Layer MoS_2 Nanoclusters. *Phys. Rev. Lett.* **2000**, *84*, 951–954.
2. Guo, Q.; Oh, W. S.; Goodman, D. W. Titanium Oxide Films Grown on Mo(110). *Surf. Sci.* **1999**, *437*, 49–60.

3. Mannig, A.; Zhao, Z.; Rosenthal, D.; Christmann, K.; Hoster, H.; Rauscher, H.; Behm, R. J. Structure and Growth of Ultrathin Titanium Oxide Films on Ru(0001). *Surf. Sci.* **2005**, *576*, 29–44.
4. Cai, T. H.; Song, Z.; Rodriguez, J. A.; Hrbek, J. Preparation and Structural Characterization of RuS_2 Nanoislands on Au(111). *J. Am. Chem. Soc.* **2004**, *126*, 8886–8887.
5. Biener, M. M.; Biener, J.; Friend, C. M. Novel Synthesis of Two-Dimensional TiS_2 Nanocrystallites on Au(111). *J. Chem. Phys.* **2005**, *122*, 034706.
6. Biener, J.; Farfan-Arribas, E.; Biener, M.; Friend, C. M.; Madix, R. J. Synthesis of TiO_2 Nanoparticles on the Au(111) Surface. *J. Chem. Phys.* **2005**, *123*, 094705.
7. Farfan-Arribas, E.; Biener, J.; Friend, C. M.; Madix, R. J. Reactivity of Methanol on TiO_2 Nanoparticles Supported on the Au(111) Surface. *Surf. Sci.* **2005**, *591*, 1–12.
8. Horn, J. M.; Song, Z.; Potapenko, D. V.; Hrbek, J.; White, M. G. Characterization of Molybdenum Carbide Nanoparticles Formed on Au(111) Using Reactive-Layer Assisted Deposition. *J. Phys. Chem. B* **2005**, *109*, 44–47.
9. Kim, J.; Dohnalek, Z.; White, J. M.; Kay, B. D. Reactive Growth of Nanoscale MgO Films by Mg Atom Deposition onto O_2 Multilayers. *J. Phys. Chem. B* **2004**, *108*, 11666–11671.
10. Kim, J.; Dohnalek, Z.; Kay, B. D. Cryogenic CO_2 Formation on Oxidized Gold Clusters Synthesized *via* Reactive Layer Assisted Deposition. *J. Am. Chem. Soc.* **2005**, *127*, 14592–14593.
11. Weaver, J. H.; Antonov, V. N. Synthesis and Patterning of Nanostructures of (Almost) Anything on Anything. *Surf. Sci.* **2004**, *557*, 1–3.
12. Song, D.; Hrbek, J.; Osgood, R. Formation of TiO_2 Nanoparticles by Reactive-Layer-Assisted Deposition and Characterization by XPS and STM. *Nano Lett.* **2005**, *5*, 1327–1332.
13. Smith, R. S.; Huang, C.; Wong, E. K. L.; Kay, B. D. Desorption and Crystallization Kinetics in Nanoscale Thin Films of Amorphous Water Ice. *Surf. Sci.* **1996**, *367*, L13−L18.
14. Verdaguer, A.; Sacha, G. M.; Bluhm, H.; Salmeron, M. Molecular Structure of Water at Interfaces: Wetting at Nanometer Scale. *Chem. Rev.* **2006**, *106*, 1478–1510.
15. Ikemiya, N.; Gewirth, A. A. Initial Stages of Water Adsorption on Au Surfaces. *J. Am. Chem. Soc.* **1997**, *119*, 9919–9920.
16. Donev, J. M. K.; Yu, Q.; Long, B. R.; Bollinger, R. K.; Fain, S. C., Jr. Noncontact Atomic Force Microscopy Studies of Ultrathin Films of Amorphous Solid Water Deposited on Au(111). *J. Chem. Phys.* **2005**, *123*, 044706.
17. Kimmel, G. A.; Petrik, N. G.; Dohnalek, Z.; Kay, B. D. Crystalline Ice Growth on Pt(111) and Pd(111): Nonwetting Growth on a Hydrophobic Water Monolayer. *J. Chem. Phys.* **2007**, *126*, 114702.
18. Smith, R. S.; Kay, B. D. The Existence of Supercooled Liquid Water at 150 K. *Nature* **1999**, *398*, 788–791.
19. Meng, S.; Kaxiras, E.; Zhang, Z. Y. Water Wettability of Close-Packed Metal Surfaces. *J. Chem. Phys.* **2007**, *127*, 244710.
20. Erb, R. A. Wettability of Gold. *J. Phys. Chem.* **1968**, *72*, 2412–2417.
21. Ogasawara, H.; Yoshinobu, J.; Kawai, M. Clustering Behavior of Water (D_2O) on Pt(111). *J. Chem. Phys.* **1999**, *111*, 7003–7009.
22. Kroes, G. J. Surface Melting of the (0001) Face of TIP4P Ice. *Surf. Sci.* **1992**, *275*, 365–382.
23. Ristenpart, W. D.; Kim, P. G.; Domingues, C.; Wan, J.; Stone, H. A. Influence of Substrate Conductivity on Circulation Reversal in Evaporating Drops. *Phys. Rev. Lett.* **2007**, *99*, 234502.
24. Kaya, S.; Sun, Y.-N.; Weissenrieder, J.; Stacchiola, D.; Shaikhutdinov, S.; Freund, H.-J. Ice-Assisted Preparation of Silica-Supported Vanadium Oxide Particles. *J. Phys. Chem. C* **2007**, *111*, 5337–5344.
25. Yan, X. M.; Ni, J.; Robbins, M.; Park, H. J.; Zhao, W.; White, J. M. Silver Nanoparticles Synthesized by Vapor Deposition onto an Ice Matrix. *J. Nanopart. Res.* **2002**, *4*, 525–533.
26. Diebold, U. The Surface Science of Titanium Dioxide. *Surf. Sci. Rep.* **2003**, *48*, 53–229.
27. Murray, P. W.; Leibsle, F. M.; Muryn, C. A.; Fisher, H. J.; Flipse, C. F. J.; Thornton, G. Interrelationship of Structural Elements on TiO_2(100)-(1 × 3). *Phys. Rev. Lett.* **1994**, *72*, 689–692.
28. Biener, M. M.; Biener, J.; Schalek, R.; Friend, C. M. Growth of Nanocrystalline MoO_3 on Au(111) Studied by *in situ* Scanning Tunneling Microscopy. *J. Chem. Phys.* **2004**, *121*, 12010–12016.
29. Lazzeri, M.; Vittadini, A.; Selloni, A. Structure and Energetics of Stoichiometric TiO_2 Anatase Surfaces. *Phys. Rev. B* **2001**, *6315*, 155409.
30. Ramamoorthy, M.; Vanderbilt, D.; Kingsmith, R. D. 1st-Principles Calculations of the Energetics of Stoichiometric TiO_2 Surfaces. *Phys. Rev. B* **1994**, *49*, 16721–16727.
31. Sedona, F.; Rizzi, G. A.; Agnoli, S.; Xamena, F.; Papageorgiou, A.; Ostermann, D.; Sambi, M.; Finetti, P.; Schierbaum, K.; Granozzi, G. Ultrathin TiO_x Films on Pt(111): a LEED, XPS, and STM Investigation. *J. Phys. Chem. B* **2005**, *109*, 24411–24426.
32. Zhang, Y.; Giordano, L.; Pacchioni, G.; Vittadini, A.; Sedona, F.; Finetti, P.; Granozzi, G. The Structure of a Stoichiometric TiO_2 Nanophase on Pt(111). *Surf. Sci.* **2007**, *601*, 3488–3496.
33. Sasaki, T.; Ebina, Y.; Kitami, Y.; Watanabe, M.; Oikawa, T. Two-Dimensional Diffraction of Molecular Nanosheet Crystallites of Titanium Oxide. *J. Phys. Chem. B* **2001**, *105*, 6116–6121.
34. Surnev, S.; Kresse, G.; Sock, M.; Ramsey, M. G.; Netzer, F. P. Surface Structures of Ultrathin Vanadium Oxide Films on Pd(111). *Surf. Sci.* **2001**, *495*, 91–106.
35. Schaub, R.; Thostrup, P.; Lopez, N.; Laegsgaard, I.; Norskov, J. K.; Besenbacher, F. Oxygen Vacancies as Active Sites for Water Dissociation on Rutile TiO_2(110). *Phys. Rev. Lett.* **2001**, *87*, 266104.
36. Sykes, E. C. H.; Tikhov, M. S.; Lambert, R. M. On the Switch Between Selective Oxidation and Selective Hydrogenation of a Terminal Alkene on Well-Defined Titania Surfaces. *Catal. Lett.* **2002**, *78*, 7–11.
37. Lide, R. D. *CRC Handbook of Chemistry and Physics*, 88 ed.; CRC Press: Cleveland, OH, 2007/2008.
38. Muller, A. D.; Muller, F.; Hietschold, M.; Demming, F.; Jersch, J.; Dickmann, K. Characterization of Electrochemically Etched Tungsten Tips for Scanning Tunneling Microscopy. *Rev. Sci. Instrum.* **1999**, *70*, 3970–3972.